JOURNAL OF Materials CHEMISTRY

SiC–SiO_x heterojunctions in nanowires

Yan Qiu Zhu,[a] Wei Bing Hu,[a] Wen Kuang Hsu,[a] Mauricio Terrones,[a] Nicole Grobert,[a] Jonathan P. Hare,[a] Harold W. Kroto,[a] David R. M. Walton*[a] and Humberto Terrones[b]

[a]*School of Chemistry, Physics and Environmental Science, University of Sussex, Brighton, UK BN1 9QJ*
[b]*Instituto de Física, UNAM, Apartado Postal, 1-1010 Querétaro, México*

Received 9th July 1999, Accepted 24th September 1999

Novel 2-D nanoscale SiC networks have been generated by heating SiC–Fe–Co mixtures under a CO atmosphere. Examination of the products by EDX and HRTEM showed that most of the nanowires consist of β-SiC elongated single crystals, wrapped in amorphous SiO_x sheaths. Intriguing crystalline features and defects associated with SiC nanowires were observed. We believe that a binary Fe–Co catalyst is responsible for the SiC network: Fe catalyses the formation of the SiC inner cores and Co the SiO_x ($x=1$–2) outer shell. A two-step growth mechanism, involving a vapour–liquid–solid (V–L–S) step, is thought to account for SiC nanowire creation.

Introduction

The discovery of carbon nanotubes has led to a dramatic revolution in nanometer-scale materials science during the 1990s.[1] Quasi one-dimensional (1-D) carbon nanotubes, carbon nanoparticles,[2] heteroatom nanotubes (*e.g.* binary B–N[3–5] and ternary B–C–N systems[6,7]) 'inorganic fullerenes',[8,9] nanorods (*e.g.* SiC, Si_3N_4 and Ga_3N_4[10,11]), nanowires (*e.g.* Si,[12–14] SiO_x,[15] Pb, Sn, Bi[16,17] and SiC[18–20]), even nanocables[21] and three-dimensional SiO_x nanoflowers,[22] have been generated successfully by various methods. These novel materials exhibit excellent mechanical properties and unique electronic behaviour.[23] SiC has attracted particular attention as a valuable semiconductor, while large SiC whiskers (*ca.* 100 μm diameter) are used in advanced composite fabrication. To date, several techniques have been developed to create SiC nanorods and nanowires, such as carbon refining,[10,18] laser ablation[21] and metal cluster-catalysed growth[24] involving V–L–S processes.[25] A recent study has shown that SiC nanorods/nanowires possess mechanical properties superior to those prevailing in the bulk form or in micrometer-size whiskers.[26] Besides its high modulus and stiffness, the strength of a SiC nanorod is close to the theoretically predicted maximum (*ca.* 600 GPa),[27] suggesting that SiC nanostructures should be excellent candidates for reinforcing ceramic, metal and polymer composites. Moreover, the electronic and mechanical properties of SiC nanorods or nanowires are strongly dependent upon their actual crystalline structures. Maximum strength may be reached for a defect-free nanowire, whereas when major defects occur (*e.g.* stacking faults or twinning) the strength is considerably reduced.[26] On the other hand, when considering such a 1-D SiC nanowire as a component of a miniature or a nanometer-sized electronic device, a well crystallised (or a predominantly defect-free) structure is extremely important. At this stage, the generation of 2-D, or even 3-D SiC nanonetworks (nanowires are interconnected by junctions in two or three dimensions) may prove to be industrially useful. For this reason, studies of the growth process and characterisation of SiC nanostructures are obviously important.

In previous experiments, we successfully produced 1-D SiC and Si nanowires, as well as 3-D SiO_x nanoflowers, by heating SiC–Fe or SiC–Co mixtures in a CO atmosphere.[28] We found that the use of Fe or Co catalysts resulted in different products: 1-D SiC nanowires and 3-D SiO_x nanoflowers,[22] respectively. With the aim of making 2- or 3-D semiconductor nanonetworks, we have now carried out experiments on an SiC–Fe–Co ternary system.

Experimental

A 5 : 1 : 1 mixture of SiC–Fe–Co† was dispersed mechanically in acetone by sonication for 10 min. The resulting suspension was transferred by pipette onto a quartz substrate ($10\times5\times1$ mm), and the acetone was allowed to evaporate, leaving a grey uniform film, *ca.* 0.5 mm thick. A foil heater ($60\times10\times0.2$ mm), constructed of high purity graphite (>99.999%), was connected securely to two graphite electrode holders, located in a water-cooled stainless steel bell jar. The quartz substrate was then heated as described previously.[22] A dc current (*ca.* 50 A) was applied to the heater until a temperature of *ca.* 1500 °C was achieved and maintained for *ca.* 40 min, then discontinued. During heating and cooling, the CO pressure was held at *ca.* 200 Torr. At the conclusion of the experiment, a sample of the light brown film was removed from the substrate and dispersed in acetone during 5 min treatment with ultrasound in a water bath. The dispersion in acetone was transferred to a copper grid, coated with holey carbon film, the acetone was allowed to evaporate and the residue was examined by transmission electron microscopy (TEM; H-7100, Phillips CM-200 and JEM-4000Fx) and energy dispersive X-ray analysis (EDX; detecting elements heavier than B).

Results

Nanowire structures

Fig. 1 shows randomly distributed nanowires. Two types can be distinguished: one has slightly larger diameters and is relatively long; the other is thinner and shorter. A large particle is usually located at the end of the nanowire, except in those cases where breakage appears to have occurred. The smaller nanowires are normally bent (Fig. 1, top left), whereas the larger ones are straighter. Both types exhibit smooth curvature under TEM. It is noteworthy that almost all of these nanowires possess a dark inner core and a lighter outer shell (<10% of the nanofibres contain no inner core). The outer diameter of the

†All starting materials were obtained from Goodfellow Ltd.: SiC: 325 mesh, >99.5% pure; Fe: <5 μm, >99.8 pure; Co: 325 mesh, >99.5% pure.

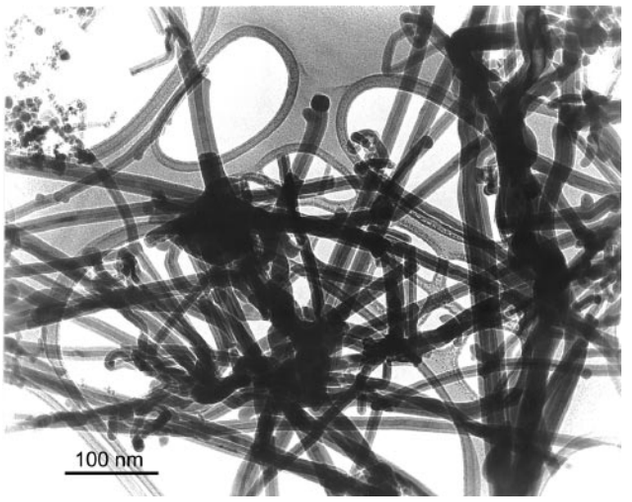

Fig. 1 TEM image of the randomly distributed nanowire/nanofibres.

outer shell lies in the range *ca.* 10–60 nm whereas that of the inner core is *ca.* 6–40 nm. Using TEM it is difficult to determine the actual length of a particular nanowire, because one end is often embedded in a densely packed area and cannot be observed adequately. Some of the nanowires are, however, extremely long: *ca.* 100 μm.

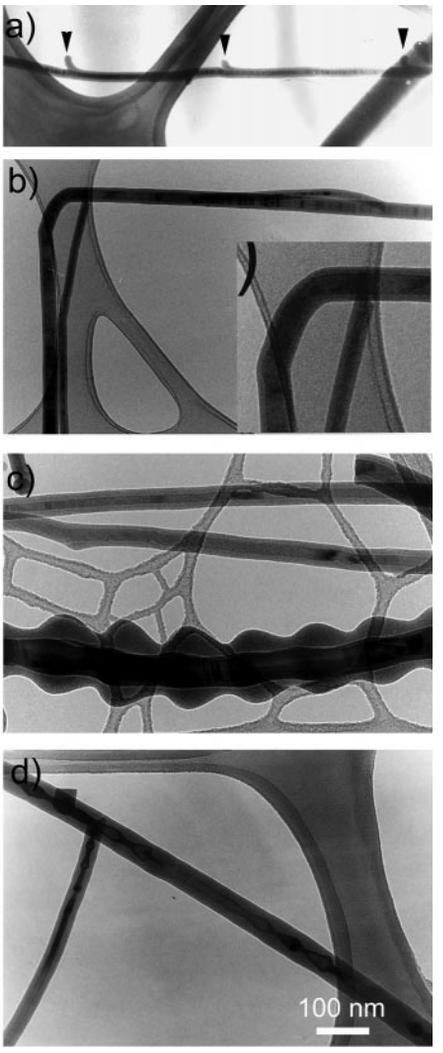

Fig. 2 TEM images: (a) a nanowire with tiny coreless protruberances (arrows), (b) a bent nanowire; the insert shows the grown facets, (c) a large nanowire with different shell diameters and (d) nanowires exhibiting variable inner cores.

Fig. 2(a) depicts a typical nanowire, of uniform diameter, with a clearly defined dark inner core (*ca.* 20 nm diameter). The three protruberances (arrowed) imply that branching has occurred. The broken branch segments appear to contain no core structure. Fig. 2(b) shows a nanowire, whose inner core and outer shell diameter are uniform. This nanowire is straight, except for a *ca.* 90° bend. The outer shell clearly shows several regular growth facets, suggesting that the bend may have occurred during the growth process, rather than as a consequence of ultrasonic treatment or the effect of acetone evaporation (during sample preparation for TEM examination). A particularly unusual nanowire [Fig. 2(c)] is significantly larger in diameter than the more abundant species. Its outer shell diameter changes considerably, but in a regular way, whereas its inner core diameter remains constant. By contrast, the outer diameter of another type of equally unusual nanowire remains constant, whereas the inner core diameter varies [Fig. 2(d)]. These observations provide fascinating examples of diverse nanostructures.

Networks

Fig. 3(a) shows a nanofibre, which appears to bifurcate at the site indicated. A similar well defined 2-D nanostructure arises from cored nanowires [Fig. 3(b)], however in this case the growing branches contain no inner cores.

Fig. 3(c) shows the layered structure of a cored 2-D nanonetwork. Robust connections between the three branches (A, B and C) may be perceived around the metal particle (O). It is noteworthy that the diameter of the metal particle is 50% greater than the diameter of each of the three branches, including their inner cores. More complex interconnections are also observed [Fig. 3(d)]. The smooth curvatures associated with the junctions suggest that these structures were actually formed during the growth process, rather than during TEM observations. Some of the junctions may be well connected

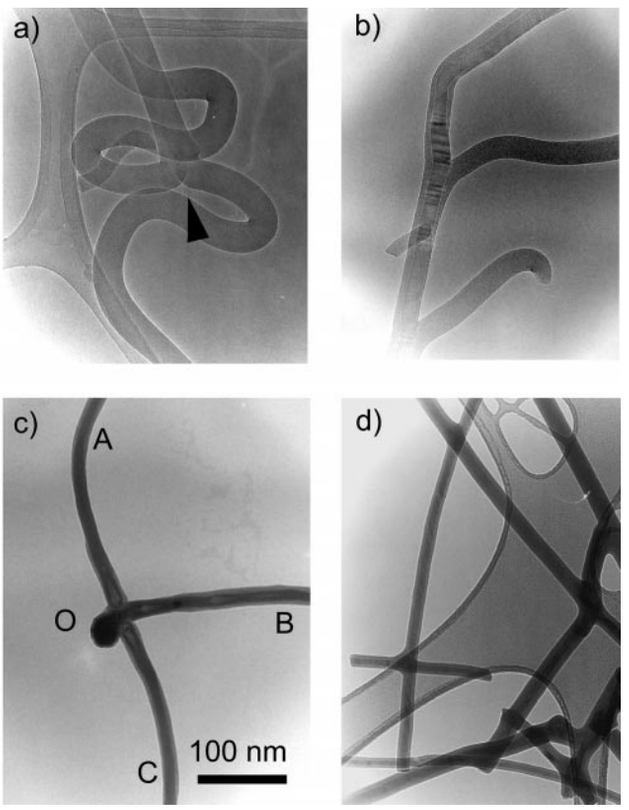

Fig. 3 TEM images: (a) 2-D structure consisting of a nanofibre, (b) 2-D structure consisting of nanowire and nanofibres, (c) a simple 2-D SiC semiconductor nanonetwork and (d) complex 2-D SiC nanonetworks.

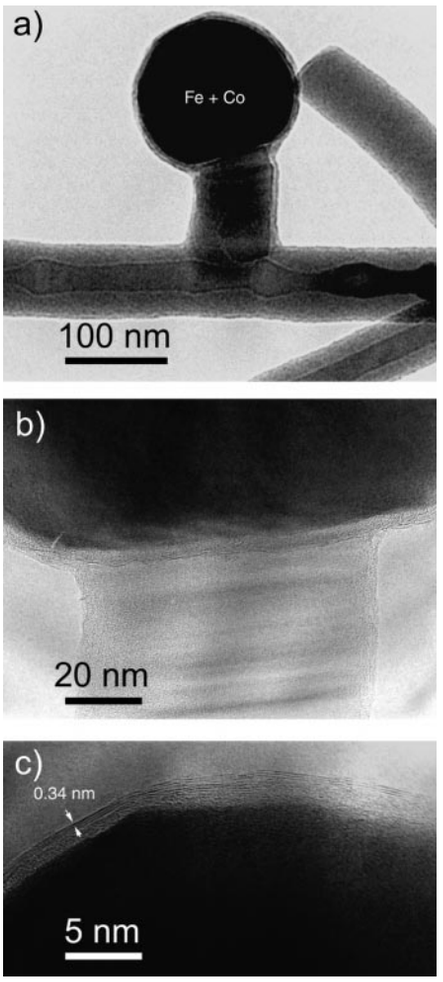

Fig. 4 (a) A typical catalytic particle, (b) the connection between the particle and the nanowire and (c) the particle covered with a partly crystallised graphitic layer.

through SiC; others may be simply bound to each other by the SiO_x (outer shells).

Metal particles are not always located at the nanowire tips. For example, a polyhedral particle, whose diameter is *ca.* twice as large as the attached nanowire, is shown in Fig. 4(a). This particle, covered with a thin layer (*vide infra*), is connected to a short nanowire with a massive inner core. The attached long nanowire, conjoined with a short branch, possesses a uniform shell and an irregular core. It seems that the inner cores are connected inside the junction. High magnification clearly reveals the existence of a thin layer covering the polyhedral particle and, importantly, a crystalline plane connected with the SiC [Fig. 4(b)]. By examining the contrast, the crystalline feature of this nanowire can easily be recognised; it is comparable to the crystalline plane of the Fe–Co catalytic particle. This metal particle is covered with partly crystallised material. The outer shell exhibits layers separated by *ca.* 0.34 nm, while the inner zone (close to the metal particle) appears to be amorphous [Fig. 4(c)]. This partly crystallised covering consists of graphitic carbon.

Composition and phases of nanowires

A series of EDX measurements was made in order to examine the different types of nanowire. The results are shown in Fig. 5. Most of the cored nanowire tips contain Fe and Co [Fig. 5(a)], whereas the tips of the coreless nanofibres consist only of Co. It appears that the EDX Fe signals are always stronger than those associated with Co for the cored nanowires. This indicates that more Fe than Co must be involved in the binary catalyst. The bulk of the nanofibres consist only of Si and O [Fig. 5(b)]. Most of the cored nanowires are composed of Si, O and C [Fig. 5(c)]; a small number of nanowires only consist of Si and O, however the Si/O ratio is much higher than that associated with nanofibres [Fig. 5(d)]. In this case, only Fe and Si were detected at the nanowire tips. Thus, the resulting materials can be typically classified as three types of composite: (1) O–Si for the nanofibres (Co at the tips), (2) Si–C–O nanowires (Fe–Co at the tips) and (3) Si–O nanowires (Fe at the tips). Further HRTEM investigations confirmed that type (1) is amorphous, the outer shells of type (2) and (3) are amorphous with the inner cores being crystalline (with a lattice fringe of *ca.* 0.25 nm, see Fig. 6) and amorphous phases, respectively. (Note that the Si and O peak intensities may differ slightly from the EDX data shown in Fig. 5, because the nanofibres and nanowires have different diameters. However, the O/Si ratio remains almost unchanged for each type of nanofibre and nanowire.)

Taking the EDX, ED and HRTEM results into account, we conclude that type (1) are amorphous SiO_x ($x=1$–2) nanofibres, type (2) are crystalline β-SiC nanowires sheathed in amorphous SiO_x ($x=1$–2) and type (3) are amorphous Si nanowires also wrapped in amorphous SiO_x ($x=1$–2).

Discussion

Chemical reactions

In previous work, we described feasible reactions whereby SiO_x and SiC might be generated in the presence of either Co or Fe.[22,28] In the present study, a binary Fe–Co (1 : 1) catalyst was used; other parameters—temperature, gas type and pressure, substrate, and heater—remained constant. Thus, reactions in each case are probably identical, the novel structural factors being associated with the growth pattern of the SiO_x and SiC nanowires. However, an interesting question may arise when we consider the thermodynamics of the Fe–Co–Si–C–O system under our experimental conditions. It seems that the most stable products will be Fe_2SiO_4 and Co_2SiO_4, plus CO_2. This result might be explained when considering the $CO:CO_2$ ratios prevailing under the reaction conditions (200 Torr CO in the reaction chamber). At high temperature (1500 °C), CO tends to act as a reducing agent and scavenges the O from the Fe and/or Co, thus suppressing Fe and/or Co oxide formation. Thus, during the reaction, Fe and/or Co remain as the reduced metals, rather than their oxides. Furthermore, acting as a reducing agent, CO also scavenges O, thereby reducing Fe_2SiO_4 and/or Co_2SiO_4 to SiO_2 and pure metals. The critical role played by CO warrants further discussion.

As regards the actual role played by Fe and Co (SiC : Fe : Co = 5 : 1 : 1), we found that large quantities of metal powders are essential for the synthesis of nanostructures. When very small amounts of Co (<1%) were used, sintered bulk SiC was produced instead of SiO_x nanofibres. This result suggests that Fe and Co may also be involved in the decomposition of SiC.

Structural features of the SiC nanowires

HRTEM was employed to investigate the detailed structure of the SiC nanowires. Most consist of single crystalline SiC cores (*ca.* 30–50 nm) with uniform SiO_x shells. Four types of nanowire cores were formed [Figs. 6(a)–(d)] differing in terms of the angles between the SiC crystalline axis and the nanowire axis (a nanowire axis is defined as the direction along the nanowire). The angles between ⟨111⟩ and the nanowire axes were measured and found to increase gradually from *ca.* 0 to 60°. This result differs somewhat from previous reports,[18–20] in which SiC micro- and/or nano-fibres were generally found to conform to Fig. 6(a). We believe that these angles reflect the direction of nanowire growth [Fig. 4(b)]. Differential crystal-

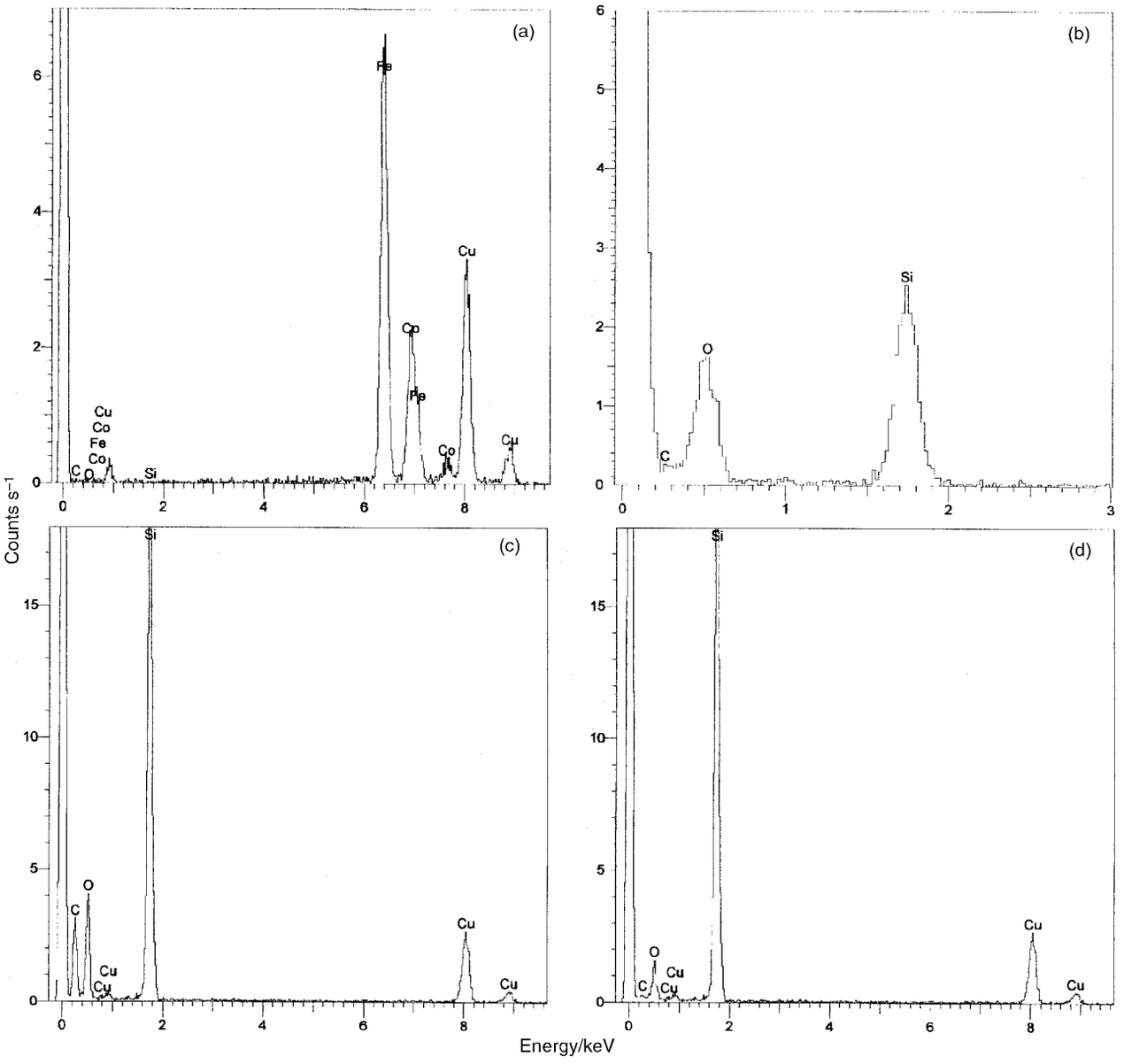

Fig. 5 EDX patterns from (a) nanowire tip (catalytic particle), (b) SiO_x nanofibre, (c) SiC nanowire and (d) Si nanowire.

line growth directions may affect the final mechanical and electronic properties of the nanowire. For example, considering the close-packed crystalline planes, {111} for SiC, the nanowire in Fig. 6(d) may possess higher tensile strength than that in Fig. 6(a), along the nanowire axis. Thus, the controlled production of nanowires with different crystalline axis directions is likely to be of considerable interest.

Nanowires exhibiting various types of growth defect have also been observed. For example, Fig. 7(a) shows a nanowire with a well crystallised SiC inner core, still a single crystal, but enclosed in an asymmetric SiO_x sheath. This phenomenon poses a question as to the nature of the dual-phase growth process associated with SiC and SiO_x. Such a structure [Fig. 7(a)] could arise if the growth rates are initially identical but then diverge. Such a feature is potentially valuable in that it is likely to facilitate connections at the resulting network junctions (Fig. 3). Fig. 7(b) shows a nanowire with two different crystalline regions, separated by the arrow. The structure (right) is a well crystallised phase, whereas that to the left contains a sequence of planar defects. From a comparison of the relationship between the atomic fringes on both sides, it is clear that they represent twin defects, probably arising from the growth process. Another type of defect consists of stacking faults [Fig. 7(c)], which may occur as a result of interior stresses arising during growth, or to external stresses arising from deformation. Note that the nanowire tends to bend (lower edge from right to left), but is probably not deformed by external forces arising during TEM examination. We suggest that these stacking faults occur during the growth process. These often happen during SiC microfibre and bulk crystal production, and are generally thought to originate from thermal stress. Therefore, the problem can normally be alleviated by annealing. During the TEM examination, we noticed that the irregular structure [Fig. 7(d)] consisted of well crystallised SiC (note the lattice fringe in the insert). However after *ca.* 5 min of electron beam irradiation (at 200 kV), this nanowire suddenly straightened and assumed a uniform diameter. Thus the effect of irradiation is similar to annealing, and reduces planar stacking defects in SiC.

Growth mechanism

The structures shown in Figs. 2–7 may grow according to a variety of mechanisms, the outcome being: *e.g.* single nanowire/nanofibres or a complex network. As regards SiO_x nanofibres with Co encapsulated at the tips (Fig. 5), we believe that the Co particle acts as a catalyst, and that nanofibre growth involves a

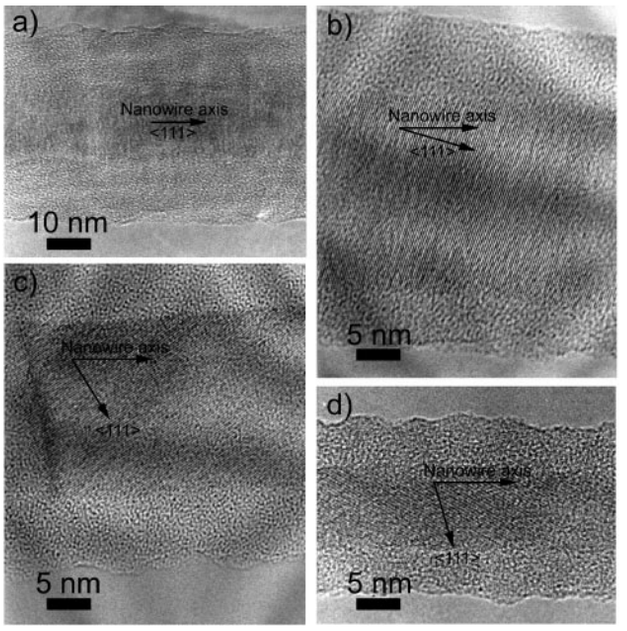

Fig. 6 HRTEM images showing four types of well crystallised SiC nanowires: from (a) to (d) the angle between the nanowire axis and the SiC ⟨111⟩ increases, from 0 to 60°. The (111) spacing is *ca.* 0.25 nm.

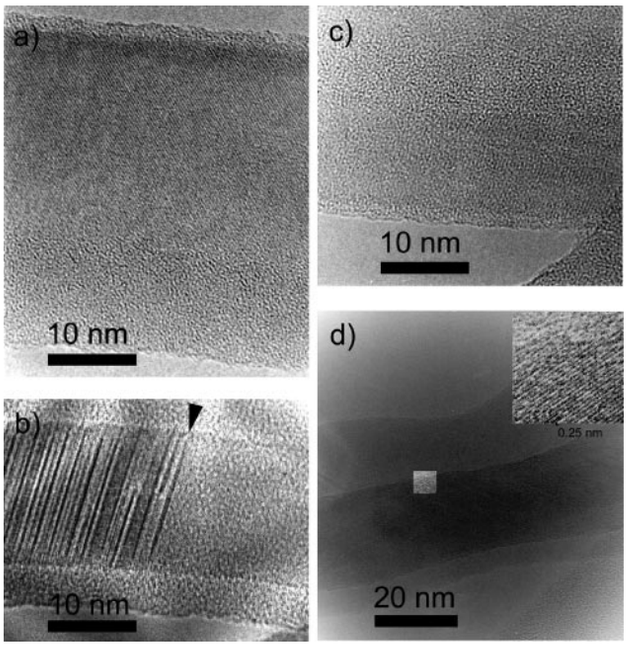

Fig. 7 HRTEM images of defective nanowire structures: (a) a well crystallised uneven nanowire, (b) twinning defects, (c) stacking default and (d) well crystallised nanowire with variable diameter.

V–L–S process.[25] During heating, vaporised SiO is absorbed by the partly molten Co (mp 1495 °C) clusters. If the concentration is high enough, Si and O then start to extrude from the Co, leading to growth of a solid nanofibre. The detailed features of this process have already been described.[22] Using pure Co as a catalyst, we often found branched growth, and we proposed a Co coalescence or bifurcation mechanism to explain this phenomenon.[29] As regards Si nanowires, produced by laser ablation, a recent report outlined a modified V–L–S mechanism associated with an Fe–Si binary system.[21] In our system, the Fe–Si–O ternary balance may well account for the production of amorphous SiO_x/Si dual-phase growth.[28] It is clear that the vapour supply at various growing stages may change, and that a particular element concentration at one specified point may change. As a result, the growth rate may fluctuate and cores or shells of different diameters may form (Figs. 2–4).

When a binary catalyst, *e.g.* Fe–Co is used, the V–L–S mechanism is still generally applicable to SiC nanowire growth. The evidence from our experiments is that carbon is adsorbed on a larger metal particle surface (Fig. 4). We can distinguish clearly between the outer graphitic layers, but not between the layers which make up the inner amorphous phase. This indicates that the pronounced absorption of Si, O and C by the metal catalyst may have destroyed the inner graphitic structures. (Note that we can only produce SiC nanowires in the presence of an iron catalyst. It seems that there is some fundamental difference between the Fe–C and Co–C catalytic action.) However, the V–L–S mechanism accounts only for amorphous nanowire growth, and not for the different shapes (defects) of the nanowires, particularly those shown in Figs. 3 and 6.

On the other hand, the notable uneven feature exhibited by SiC nanowires [Fig. 7(a)] may suggest an alternative growth process. It is obvious that a dual-phase eutectic-type growth is unlikely, because the amorphous SiO_x phase does not bear any crystalline relationship to SiC in our case. We therefore propose a two-step growth mechanism for uneven SiC nanowires, based on the V–L–S mechanism. It is likely that SiC starts to nucleate and crystallise along with Si and C extrusion from the catalyst. A uniform SiC nanowire (covered with a thin SiO_x layer, following the V–L–S mechanism[25]) then forms in a first step. During this stage, the crystallisation process is analogous to the general re-crystallisation phenomenon brought about by annealing. In some cases, when the second stage takes place, crystallisation may still be incomplete, for various reasons (such as low temperature). Therefore, unstable or defective structures may be removed by thermal annealing or by electron irradiation under the microscope. The electron beam irradiation results associated with Fig. 7(d) support this analysis. As mentioned above, the shape of the catalytic particle strongly affects the resulting nanowires [Fig. 3(d)], as well as their crystalline planes (Fig. 4). This phenomenon is similar to metal-catalysed carbon fibre growth, as described by Baker.[30] It is most likely that SiC nucleates on the surface of the attached catalyst. In consideration of the crystalline plane mismatch between the catalyst and SiC, various Fe–Co combinations are likely to slightly alter the *d*-spacing of the catalyst and then be matched by proper SiC crystal planes. As a result, crystalline growth occurs in various directions (Fig. 6). It is possible to control the direction of SiC nanowire growth by choosing the metal catalyst with a specified *d*-spacing. After such a SiC template is obtained, SiO vapour may accumulate directly on the outer SiO_x layer of the nanowire (rather than on the catalytic particle), the second step. The first step determines the final SiC core structure, whereas the second results only in SiO_x shell thickening. Thus, uniform deposition leads to a symmetric nanowire, whereas uneven deposition in turn results in an asymmetric nanowire.

Because of the presence of Co in the catalytic particle (owing to melting or diffusion of Co and Fe during heating), the branched growth may easily occur (following a similar bifurcation stage). So does a junction (following a coalescence mechanism).[29] During nanowire growth, when the growing Fe–Co tip meets another nanowire, the nanowires may join [growth either stops, as in Fig. 3(d), or continues to grow as in Fig. 3(d)], leading to a SiC nanonetwork. We propose that these interesting nanonetworks arise from the binary catalyst: Co appears to be responsible for the junctions and Fe for the SiC nanowires. At this stage, it is still not clear why and how Co works in this way. It is possible that the *in situ* grown 2-D networks may possess better mechanical properties than those woven from fibres. So far, we have no direct evidence for the connection of SiC at the junctions, however the uneven SiO_x coating [Fig. 7(a)] and re-crystallisation by annealing for SiC

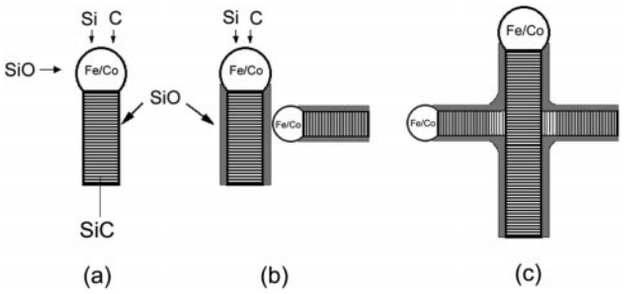

Fig. 8 A schematic model illustrating the nanowire growth: (a) the growth of SiC central core, (b) thickening of the nanowire and (c) formation of a network.

could establish connections at the junctions. Measurements of the electronic behaviour displayed by such tiny semiconductor networks constitute an interesting challenge for the future.

On the basis of the above discussion, we propose a model to account for the nanowire network growth affected by the catalysts (Fig. 8). Fig. 8(a) illustrates the deposition of SiO, Si and C on the Fe or Fe–Co surface, leading to SiC nanowire growth, the first step. After the formation of the SiC core, further SiO deposition on the surface of the nanowire thickens the SiO_x outer shell, the second step [Fig. 8(b)]. At the same time, another nanowire grows towards it, and an interconnected network is created [Fig. 8(c)].

Summary

Here, we have described the generation of 1-D nanowires/nanofibres, particularly novel 2-D semiconductor nanonetworks, using a binary Fe–Co catalyst. Nanofibre formation is believed to be catalysed by a single Co particle, the Si nanowire by a single Fe particle, and the majority of SiC nanowires by a binary Fe–Co catalyst. Comprehensive HRTEM investigations have revealed that most nanowires consist of well crystallised β-SiC elongated (<100 μm) single crystals, wrapped in an amorphous SiO_x ($x=1$–2) sheath. A series of crystalline features and defects associated with SiC nanowires has been presented. Based on experimental results, we propose a two-step growth mechanism in conjunction with the V–L–S process for SiC nanowires. We believe that the binary Fe–Co catalyst is responsible for SiC network growth. The 1-D nanowire and the novel 2-D network may be useful for advanced composite material fabrication and in the electronics industry.

Acknowledgements

We thank the Royal Society (Y.Q.Z., W.K.H.), the Mexican Academy of Sciences (H.T.), Japanese Fine Ceramic Center (N.G., Y.Q.Z.), Conacyt-México (H.T.), and the EPSRC (M.T.) for financial support. We are grateful to L. Rendón (UNAM), and to J. Thorpe and D. Randall (Sussex) for assistance with TEM facilities.

References

1 S. Iijima, *Nature (London)*, 1991, **354**, 56.
2 D. Ugarte, *Nature (London)*, 1992, **359**, 707.
3 N. G. Chopra, R. J. Luken, K. Cherry, V. H. Crespi, M. L. Cohen, S. G. Louie and A. Zettl, *Science*, 1995, **269**, 966.
4 M. Terrones, W. K. Hsu, H. Terrones, J. P. Zhang, S. Romas, J. P. Hare, R. Castillo, K. Prassides, A. K. Cheethham, H. W. Kroto and D. R. M. Walton, *Chem. Phys. Lett.*, 1996, **259**, 568.
5 D. Goldberg, Y. Bando, M. Eremets, K. Takemura, K. Kurashima, K. Tamiya and H. Yusa, *Chem. Phys. Lett.*, 1997, **279**, 191.
6 O. Stephan, P. M. Ajayan, C. Colliex, P. Redlich, J. M. Lambert, P. Bernier and P. Lefin, *Science*, 1994, **266**, 1683.
7 Y. Zhang, H. Gu, K. Suenaga and S. Iijima, *Chem. Phys. Lett.*, 1997, **279**, 264.
8 R. Tenne, L. Margulis, M. Genut and G. Hodes, *Nature (London)*, 1992, **360**, 444.
9 L. Margulis, G. Salitra, R. Tenne and M. Talianke, *Nature (London)*, 1993, **365**, 113.
10 H. Dai, E. W. Wong, Y. Z. Lu, S. Fan and C. M. Lieber, *Nature (London)*, 1995, **375**, 769.
11 W. Han, S. Fan, Q. Li and Y. Hu, *Science*, 1997, **277**, 1287.
12 G. D. Saunders and Y. C. Chang, *Phys. Rev. B: Condens. Matter*, 1992, **45**, 9202.
13 A. M. Morales and C. M. Lieber, *Science*, 1998, **279**, 208.
14 N. Wang, Y. H. Tang, Y. F. Zhang, C. S. Lee, I. Bello and S. T. Lee, *Chem. Phys. Lett.*, 1999, **299**, 237.
15 D. P. Yu, Q. L. Hang, Y. Ding, H. Z. Zhang, Z. G. Bai, J. J. Wang, Y. H. Zou, W. Qian, G. C. Xiong and S. Q. Feng, *Appl. Phys. Lett.*, 1998, **73**, 3076.
16 W. K. Hsu, M. Terrones, H. Terrones, N. Grobert, A. I. Kirkland, J. P. Hare, K. Prassides, P. D. Townsend, H. W. Kroto and D. R. M. Walton, *Chem. Phys. Lett.*, 1998, **284**, 177.
17 W. K. Hsu, J. Li, H. Terrones, M. Terrones, N. Grobert, Y. Q. Zhu, S. Trasobares, J. P. Hare, C. J. Pickett, H. W. Kroto and D. R. M. Walton, *Chem. Phys. Lett.*, 1999, **301**, 159.
18 D. Zhou and S. Seraphin, *Chem. Phys. Lett.*, 1994, **222**, 233.
19 G. W. Meng, L. D. Zhang, C. M. Mo, S. Y. Zhang, Y. Qin, S. P. Feng and H. J. Li, *J. Mater. Res.*, 1998, **13**, 2533.
20 G. W. Meng, L. D. Zhang, Y. Qin, F. Phillipp, S. R. Qiao, H. M. Guo and S. Y. Zhang, *Chin. Phys. Lett.*, 1998, **15**, 689.
21 Y. Zhang, K. Suenaga, C. Colliex and S. Iijima, *Science*, 1998, **281**, 97.
22 Y. Q. Zhu, W. K. Hsu, M. Terrones, N. Grobert, H. Terrones, J. P. Hare, H. W. Kroto and D. R. M. Walton, *J. Mater. Chem.*, 1998, **8**, 1859.
23 M. Terrones, W. K. Hsu, H. W. Kroto and D. R. M. Walton, *Top. Curr. Chem.*, 1999, **199**, 190.
24 J. V. Milewski, F. D. Gac, J. J. Petrovic and S. R. Skaggs, *J. Mater. Sci.*, 1985, **20**, 1160.
25 R. S. Wanger and W. C. Ellis, *Appl. Phys. Lett.*, 1964, **4**, 39.
26 E. W. Wong, P. E. Sheehan and C. M. Lieber, *Science*, 1997, **277**, 1971.
27 N. H. Macmillan, *J. Mater. Sci.*, 1972, **7**, 239.
28 Y. Q. Zhu, W. B. Hu, W. K. Hsu, M. Terrones, N. Grobert, T. Karali, H. Terrones, J. P. Hare, P. D. Townsend, H. W. Kroto and D. R. M. Walton, *Adv. Mater.*, 1999, **11**, 844.
29 Y. Q. Zhu, W. K. Hsu, M. Terrones, N. Grobert, W. B. Hu, J. P. Hare, H. W. Kroto, D. R. M. Walton and H. Terrones, *Chem. Mater.*, in press.
30 R. T. K. Baker, *Carbon*, 1989, **27**, 315.

Paper 9/05547I